Photoabsorption and photoion spectroscopy of atomic uranium in the region of $6p$ and $5d$ excitations

P. van Kampen,[1] Ch. Gerth,[1,2] M. Martins,[3] P. K. Carroll,[4] J. Hirsch,[1] E. T. Kennedy,[1] O. Meighan,[1] J.-P. Mosnier,[1] P. Zimmermann,[2] and J. T. Costello[1]

[1]*Centre for Laser Plasma Research, National Centre for Plasma Science and Technology, School of Physical Sciences, Dublin City University, Dublin 9, Ireland*

[2]*Institut für Atomare und Analytische Physik, Hardenbergstrasse 36, Technische Universität Berlin, D-10623 Berlin, Germany*

[3]*Institut für Experimentalphysik, Freie Universität Berlin, Arnimallee 14, D-14195 Berlin, Germany*

[4]*Department of Experimental Physics, National University of Dublin, Belfield, Dublin 4, Ireland*

(Received 18 January 2000; published 10 May 2000)

The photoabsorption process in atomic uranium has been investigated experimentally and theoretically in the 15–150-eV region. Using the dual laser plasma technique, the $6p$ photoabsorption spectrum has been recorded while for the first time the $5d$ region has been remeasured photoelectrically using both photoabsorption and photoion spectroscopy. Interpretation of the photoabsorption spectra is supported by Hartree-Fock calculations which take into account spin-flip decay and the interaction of many discrete states with many continua. The $6p$ spectrum is entirely dominated by spin-orbit split $6p \rightarrow 6d$ transitions. The $5d$-subshell photoabsorption is shown to consist predominantly of discrete $5d \rightarrow 5f$ excitations; here the electrostatic and spin-orbit interactions are comparable in strength.

PACS number(s): 32.80.Fb

I. INTRODUCTION

A knowledge of the properties of the actinides is of fundamental interest to both physics and chemistry, and the field of actinide research spans a wide range of scientific disciplines. The key to gaining a deeper insight into the physics and chemistry of actinide elements lies with understanding the behavior of the $5f$ wave function. Its homolog counterpart, the $4f$ wave function in the lanthanides, is becoming increasingly well understood: the $4f$ electron experiences a double-well potential whose detailed properties are term dependent. With increasing atomic number Z or degree of ionization ζ, all terms of the $4f$ wave function eventually collapse into the inner well which renders the $4f$ electron localized and chemically inert. While $5f$ electrons in the actinides also experience a double-well potential, they can never be localized to the same extent as the $4f$ electrons in the lanthanides due to the additional node in the $5f$ wave function. Many of the atomic and solid-state properties peculiar to the actinides can be attributed to this fact [1].

Photoabsorption is a selective tool for the investigation of atomic structure in the VUV and XUV regions since dipole transitions dominate virtually to the exclusion of other multipole transitions and thus a simplified set of data is obtained. Due to the potential radiological hazards and scarcity of many of the actinides, however, the only experimental VUV and XUV photoabsorption data on actinide atoms available to date are those of thorium in the 15–150-eV range [2,3] and uranium in the 80–150-eV range [4,5]; data are also available for solids and molecules containing these two elements [6–8]. An extensive list of references for spectroscopic data on actinide elements, which includes other spectral regions, is given by Blaise and Wyart [9].

No supporting experimental data, such as photoelectron or photoion data, on actinide atoms are available. However, x-ray photoabsorption data exist for a film of uranium metal recorded by Fuggle *et al.* [10] from which ionization limits were extracted for solid uranium. Optical constants and cross sections evaluated using fast electron-energy-loss spectroscopy are provided in [11,12].

From a theoretical perspective, the complex photoabsorption spectra of uranium reflect the intershell coupling of the $6p$ and $5d$ core holes with the open $5f$ and $6d$ subshells; they constitute therefore stringent test cases for sophisticated many-electron calculations. The local-density–random-phase approximation (LDRPA) has been used by Wendin [13] and Wendin and Kerr del Grande [14] to compute the uranium photoionization cross section. According to the LDRPA calculations, there is a tall narrow feature at about 94 eV that lies entirely below the $5d_{5/2}^{-1}$-limit at 102 eV, while the $5d_{3/2}^{-1}$-limit lies just above the peak of, but well within, a second broad feature at higher energy. Zangwill and Liberman carried out atomic calculations within the framework of the relativistic time-dependent local-density approximation (RTDLDA) in the 90–120-eV region and found the peaks to lie at 96 and 104 eV [15].

In this paper we present the results of an extensive study of photoabsorption by atomic uranium in the 15–150-eV region. The $6p$-subshell photoabsorption has been measured for the first time while the $5d$ region has been remeasured using both photoabsorption and photoion spectroscopy. Reproduction and interpretation of the spectrum is achieved within the framework of the extended Fano theory by the application of the Mies formalism [16] which takes into account the interaction of many discrete states with many continua.

II. EXPERIMENT

Photoabsorption experiments were performed in the VUV (15–40 eV) and XUV (40–150 eV) regions using the dual laser plasma (DLP) technique (Refs. [3,17–20] and refer-

ences therein) at the Centre for Laser Plasma Research at Dublin City University. In the DLP experiments, a laser-produced tungsten plasma was used to backlight a uranium plasma created by a 25-ns, 1.5-J *Q*-switched ruby laser focused to a power density of $\approx 10^8$ Wcm^{-2}. The spectra were recorded on a 1-m normal incidence spectrometer with a resolving power of ≈ 800 in the 15–40-eV region and on a 2.2-m grazing incidence spectrometer in the 30–150-eV region with a resolving power of 1200–2500. The spectra overlapped in the 30–40-eV photon-energy range which provided verification that the data were recorded under identical plasma conditions.

The XUV-DLP system samples a square element of the absorbing plasma approximately 250×250 μm^2 in size. In the VUV-DLP experiment an area of 500×500 μm^2 was selected to be sampled by the insertion of a preslit. In both cases the sampled volume was chosen to lie at a distance of 2.0 mm from the uranium target surface. We recorded a series of uranium plasma photoabsorption spectra at interplasma delays ranging from 150 to 2500 ns. At short time delays, some distinct narrow features superimposed on broad resonances were observed. However, at time delays of more than 600 ns the shape of the spectrum no longer changed, indicating that an end point had been reached in evolution from ionic via ionic-atomic to exclusively atomic absorption.

Regarding the experimental difficulty of oxidation of the target surface, the DLP technique offers a distinct advantage compared to other techniques. As described by Fuggle *et al.* [10], a uranium metal surface oxidizes at pressures as low as 10^{-6} mbar, which would be the typical pressure in our experiment. A few laser pulses fired before recording the absorption data, however, remove any possible surface oxidation since they atomize any uranium oxides formed.

The temperature of the uranium plasma was such that no XUV emission was observed, but in the VUV-DLP experiments a small but detectable emission signal was recorded. To take this emission as well as dark current effects into account, the VUV-DLP experiment was conducted as follows. For each wavelength setting of the spectrometer the following four spectra were recorded: I_{cont}, the continuum emission signal obtained from the tungsten plasma; I_{trans}, the signal transmitted through the absorbing uranium plasma; I_{front}, the uranium plasma emission signal; and I_{dark}, the signal measured in the absence of any plasma. The dark current I_{dark} was typically less than 10% of I_{cont} and I_{trans} while the recorded uranium plasma emission I_{front} was $\approx 1.05 I_{\mathrm{dark}}$.

The true continuum emission I_0 is equal to I_{cont}-I_{dark}, while the true absorption signal I is given by $I = I_{\mathrm{trans}} - I_{\mathrm{front}}$ (since I_{front} includes the dark current). The absorbance σ^* was evaluated using the following equation:

$$\sigma^* = \ln\left(\frac{I_0}{I}\right) = \ln\left(\frac{I_{\mathrm{cont}} - I_{\mathrm{dark}}}{I_{\mathrm{trans}} - I_{\mathrm{front}}}\right). \tag{1}$$

A similar procedure was followed to evaluate the absorbance in the XUV-DLP experiments, the only difference being that I_{front} was replaced by I_{dark} in Eq. 1. We also note that I_{dark} is much lower than in the VUV experiment, typically less than 1% of I_{cont}. If the uranium plasma is optically thin, we may equate the absorbance to the relative photoabsorption cross section $\sigma \int_0^l n(l')\mathrm{d}l'$ according to Lambert-Beer's law (where n, the number density, is integrated along the absorbing column of length l). Where the absorbance is of the order of unity or higher, the relative photoabsorption cross section tends to be somewhat higher than σ^*.

Photoion data were obtained in the 80–140-eV region using synchrotron radiation from the electron storage ring BESSY I. The synchrotron radiation was dispersed by a toroidal grating monochromator (TGM) and focused on the atomic beam, which was produced in an effusion oven heated by electron impact [21]. The uranium metal was contained in a molybdenum crucible. A temperature of about 2500 K is necessary for the thermal evaporation of uranium to yield a sufficient number density in the interaction region ($\approx 10^{11}$ cm^{-3}). Due to this high temperature the crucible could be used for only 4 h before it disintegrated.

The photoion spectra were recorded at the beamline TGM 3 with a resolving power of $E/\Delta E \approx 200$. The photoions were extracted from the interaction region by short electric pulses (5 μs, -120 V), which were also used as start pulses in a standard time-of-flight measurement with a Wiley-McLaren-type spectrometer [22]. The ions were postaccelerated onto a microchannel plate (MCP) by a voltage of 4 keV between the drift tube and the MCP. It has been verified that for lower-Z elements the detection efficiency does not depend on the charge state, but we have not been able to establish this for uranium due to the short period that the experiment was running. By setting appropriate time windows for the stop pulses from the ion detector, the photoion yield spectra of singly to quadruply charged ions were measured simultaneously as a function of the photon energy.

III. RESULTS AND DISCUSSION

The photoabsorption spectrum of laser-produced atomic uranium in the 15–150 eV photon energy range is shown in Fig. 1. The two prominent structures between 20 and 40 eV are due to $6p$ photoabsorption; the peaks at 97.5 and 110 eV result from photoabsorption from the $5d$ subshell. In the 40–90-eV region the photoabsorption cross section decreases smoothly and monotonically, thus no features associated with the $6s$-subshell photoabsorption were discernible in these experiments.

Also shown in Fig. 1 are calculated spectra for the regions of $6p$ and $5d$ photoabsorption that will be discussed in detail below. Here we note that the relative heights of all four peaks are reproduced well, especially when we allow for the fact that for high values of σ^* the absorbance is likely to underestimate the relative photoabsorption cross section.

A. The $6p$ region

Figure 2(a) shows an expanded view of the photoabsorption spectrum of atomic uranium in the region of the $6p$ excitations. The spectrum is dominated by two strong peaks: a higher, narrower, and more symmetric peak at 21.5 eV and a broader asymmetric feature reaching its maximum at 30.5 eV.

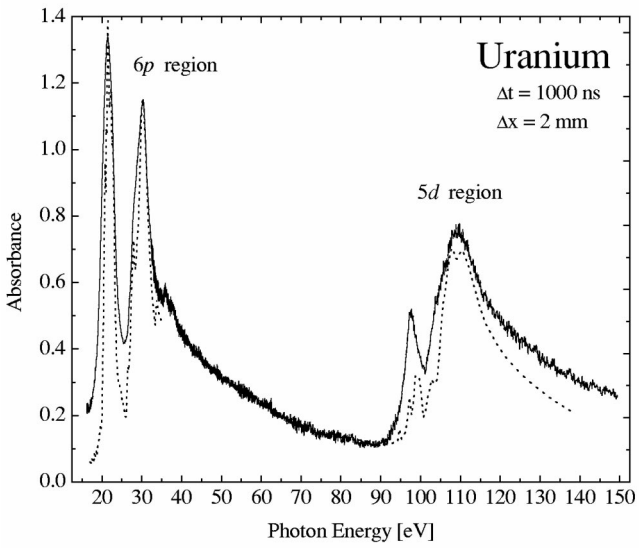

FIG. 1. Experimental and calculated photoabsorption spectra of uranium in the 15–150-eV region. The calculated spectra have been offset to compensate for the omission of direct photoionization from lower-lying subshells, but have not been adjusted otherwise. An absolute scale is given in Figs. 2 and 3.

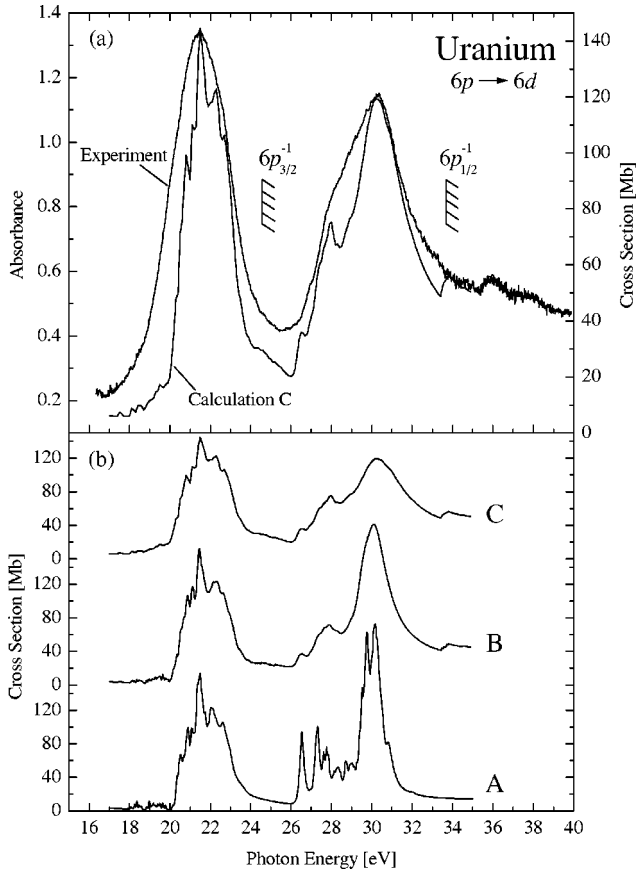

FIG. 2. Photoabsorption spectra of atomic uranium in the $6p$ region: (a) experiment and final calculation *C*; (b) final calculation *C* with intermediate calculations *A* and *B*. The arced lines denote the lowest $6p_{3/2}^{-1}$ and $6p_{1/2}^{-1}$ thresholds.

To interpret the experimental spectra we calculated the photoabsorption spectrum of atomic uranium using the Cowan code [23]. As is customary in Cowan code calculations of spectra of atomic species, the calculated Slater F_k, G_k, and R_k integrals were reduced to 85% of their *ab initio* values to account for interaction with high-lying configurations omitted from the calculation while the *ab initio* values of the spin parameter ζ_{nl} were retained. The final results of these calculations of the photoabsorption cross section in the $6p$ region are also shown in Fig. 2(a) together with the lowest $6p_{3/2}^{-1}$ and $6p_{1/2}^{-1}$ thresholds. We illustrate the physical processes which lead to the two observed peaks with two simpler intermediate calculations before discussing the final calculation. The results of these three sets of calculations are shown in Fig. 2(b).

The same initial-state configurations were used in all three sets of calculations. Ideally, the ground-state configuration of uranium should be described as [Rn] $(5f6d7s)^6$, and all possible distributions of six electrons among the $5f$, $6d$, and $7s$ subshells should be considered. However, these can be coupled in so many different ways that inclusion of all permutations becomes computationally intractable. Fortunately, the lowest odd-parity states of uranium all have the same electron configuration, $5f^3 6d7s^2$, and in each case the $6d$ and $7s$ wave functions are coupled to the $5f^3\ ^4I$ parent state. We have carried out calculations for the six lowest odd-parity states of uranium: the [Rn] $5f^3(^4I)6d7s^2\ ^5L_6$ ground state and the $^5K_5$, $^5L_7$, $^5H_3$, $^5K_6$, and $^5I_4$ states. This selection covers all states of energies within 0.7 eV from the ground state [9], which are the most likely states to be populated within the plasma; however, the results of the calculations and therefore the interpretation of the spectrum do not depend critically on the inclusion or omission of states above 0.4 eV. The results of all calculations are presented as a weighted sum of the photoabsorption cross sections from each of these initial states; the weighting factor is the multiplicity $(2J+1)$.

In the simplest set of calculations, *A*, $6p \rightarrow 6d$ transitions were the only discrete excitations included. Independent autoionization decay of these excitations was also taken into account to obtain estimates of the width of each spectral line. As for calculations of the ground state, restrictions had to be applied to the open $5f$ shells occurring in the excited state configurations. Of states with three $5f$ electrons, only the ^4I term was selected and states with two $5f$ electrons were limited to the triplet terms ^3P, ^3F, ^3H. Each of these $5f^n$ terms is coupled to the underlying core hole and all other open subshells.

These calculations, shown in curve *A* of Fig. 2(b), predict two sets of peaks. Both peaks exhibit Fano profiles [24] which reflects interference with direct autoionization into identical continuum states. The first set of peaks (at lower energies) is in reasonable agreement with experiment, but the second group of peaks is neither wide nor smooth enough and is predicted to be too tall.

Nonetheless some important conclusions can be drawn from these calculations. The separation of the $6p$ excitations into two groups of resonances can be attributed to the spin-orbit splitting of the $6p$ core hole. The first group of reso-

TABLE I. The initial and final states used to calculate the photoabsorption spectrum of atomic uranium in the region of the $6p$ excitations. The two-hole notation in the second column denotes autoionization from the $6p^5 5f^3 6d^2 7s^2$ state whereby one of the electrons fills the $6p$ core hole while the other is ejected. Interaction with direct ionization leading to identical states is accounted for.

Type of configuration	Transition(s)	Configuration(s)
Initial states		$6p^6 5f^3 6d 7s^2$
Discrete excited states	$6p \rightarrow 6d$	$6p^5 5f^3 6d^2 7s^2$
Direct $6p$ ionization	$6p \rightarrow \varepsilon s,d$	$6p^5 5f^3 6d 7s^2 + \varepsilon s,d$
Autoionization	$6d^{-2}$	$6p^6 5f^3 7s^2 + \varepsilon p,f$
	$6d^{-1}7s^{-1}$	$6p^6 5f^3 6d 7s + \varepsilon p,f$
	$5f^{-2}$	$6p^6 5f 6d^2 7s^2 + \varepsilon p,f$
	$5f^{-1}6d^{-1}$	$6p^6 5f^2 6d 7s^2 + \varepsilon d,g$
	$5f^{-1}7s^{-1}$	$6p^6 5f^2 6d^2 7s + \varepsilon s,d,g$

nances around 21.5 eV can be ascribed to $6p_{3/2} \rightarrow 6d$ transitions; the second group, around 30 eV, is due to $6p_{1/2} \rightarrow 6d$ transitions. It is clear that the calculation for the high-energy peak disagrees with experiment due to the omission of an important decay mechanism which further broadens the $6p_{1/2} \rightarrow 6d$ transitions.

All resonantly excited $6p \rightarrow 6d$ states may autoionize into the $5f$, $6d$, and $7s$ continua. Since all of the excited $6p_{1/2} \rightarrow 6d$ states are located above the $6p_{3/2}^{-1}$ ionization limits they may also decay to $6p_{3/2}^{-1}$ continuum states by the process

$$6p_{1/2}^{-1} 5f^3 6d^2 7s^2 \rightarrow 6p_{3/2}^{-1} 5f^3 6d 7s^2 + \varepsilon s,d.$$

This additional decay mechanism with a spin-flip of the $6p_{1/2}^{-1}$ core hole, omitted from calculation *A*, was taken into account in calculation *B* by inclusion of the $6p^5 5f^3 6d 7s^2 + \varepsilon s,d$ configurations. This spin-flip decay explains why the observed high-energy peak is lower and broader than the low-energy peak. (A similar mechanism has already been proposed to represent the dominant decay process of the $5p_{1/2} \rightarrow 5d$ resonances in Yb [25] and Lu [26].) As shown in Fig. 2(b), both calculated peaks become wider and smoother and agreement between experiment and calculation is improved markedly for the high-energy peak. Calculation *B* also brings out the $6p_{1/2}^{-1}$-limits above 33 eV.

Comparison of these experimental and theoretical results indicates that the resonances overlap considerably; they should therefore not be treated as independent but as resonances interacting with each other via coupling with the corresponding continua. To account for this interaction of many states with many continua we have applied the so-called extended Fano theory within the Mies formalism in calculation *C*, which results in the further broadening of both $6p \rightarrow 6d$ resonances. Initial and final states included in calculation *C* are listed in Table I.

As can be seen from Fig. 2(a), the profile of the calculated spectrum *C* is, broadly speaking, in good agreement with the experimental spectrum despite the restricted basis set used; hence the calculations allow us to interpret the nature of the peaks as follows. The $6p$ excitations are spin-orbit split by ≈ 9 eV into a group of $6p_{3/2} \rightarrow 6d$ resonances around 21.5 eV and a group of $6p_{1/2} \rightarrow 6d$ excitations around 30 eV. Due to the electrostatic intershell interaction of the $6p$ core hole with the open $5f$ and $6d$ shells, each of the smooth peaks is the result of a multitude of unresolved transitions from many different initial states merging together; instrumental broadening is negligible. In addition to the strong resonances there is evidence of up to three features between 33 and 36 eV that we ascribe to the $6p_{1/2}^{-1}$ ionization limits. The $6p_{3/2}^{-1}$ limits are completely submerged within the $6p_{1/2} \rightarrow 6d$ peak.

The photoabsorption spectra of uranium and thorium are quite similar in appearance: the $6p$ photoabsorption spectrum of thorium exhibits the same distinct spin-orbit splitting into two peaks (in this case centered at photon energies of 20.6 and 27.2 eV) [2]. Thorium has atomic number $Z=90$ and a ground-state configuration [Rn] $5f^0 6d^2 7s^2$, and yet the center of the uranium $6p_{3/2} \rightarrow 6d$ resonance lies only 1-eV higher than that of thorium; this indicates that, in going from thorium to uranium, the increase in core charge is almost entirely compensated for by the shielding effect of the $5f$ electrons.

B. The $5d$ region

The experimental photoabsorption spectrum of atomic uranium in the region of $5d$ photoexcitation is shown in Fig. 3(a). The current DLP data obtained photoelectrically are in good general agreement with the DLP data derived from photographic plates [5]. The weak shoulder on the high-energy side of the photographic data, which was attributed to residual ionic photoabsorption, is absent in the current photoelectric data.

The profile of the $5d$ resonance is Fano-like and does not look like a shape resonance as found, e.g., in the $4d$ photoabsorption spectra of Xe, Cs, and Ba [27]. In contrast to the $6p$ case, the two overlapping peaks in the $5d$ region are not exclusively due to spin-orbit splitting. Our calculations reveal that the $5d$-$5f$ electrostatic and spin-orbit terms are of comparable importance. A similar finding has been made by Wendin using the LDRPA model [13].

We carried out extensive Hartree-Fock (HF) calculations for the $5d \rightarrow 5f$ excitations similar to those for the $6p \rightarrow 6d$ resonances. The configurations included in these calculations are listed in Table II; the results are shown in Fig. 3. The same restrictions on configurations with two or three $5f$ electrons apply; configurations with four $5f$ electrons are restricted to ^5I, ^5G, ^3M, ^3L, $^3K1$, $^3K2$, $^3I1$, and $^3I2$ coupled to other open subshells. As before it was found necessary to include both the spin-flip decay channels and to use the Mies formalism to obtain good agreement with experiment. In contrast to the $6p$ calculations it was necessary to shift the computed $5d$ cross sections to lower energy by 2 eV to obtain better agreement between experiment and calculation, presumably due to the omission of states where one or both of the $7s$ electrons is replaced by $6d$.

Once again, notwithstanding the restrictions on the discrete basis states used, the computed cross section is in very good agreement with the experimental spectrum as shown in

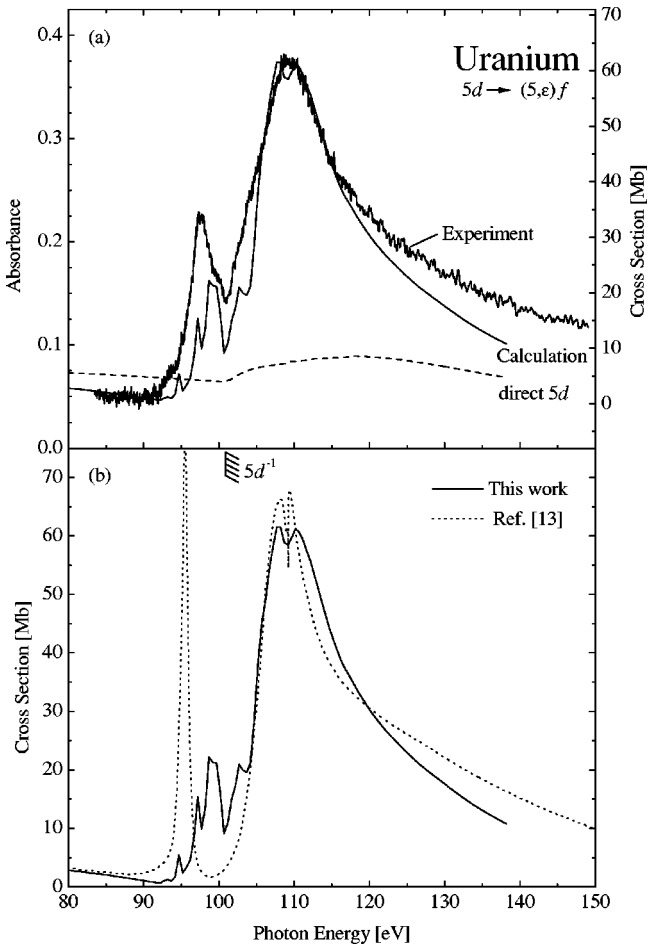

FIG. 3. Experimental and calculated photoabsorption spectra of atomic uranium in the $5d$ region: (a) experiment, full calculation (solid line) and calculation for direct $5d$ ionization only (dashed line); (b) comparison of the present calculation and that of Ref. [13]. The arced lines denote the lowest $5d^{-1}$ threshold. The calculated cross section is displayed in such a way that the 0-Mb level coincides with the experimental spectrum at the onset of $5d$ ionization to compensate for the omission of direct photoionization from lower-lying subshells.

Fig. 3(a). Comparing the present calculation with the LDRPA calculation by Wendin [13] in Fig. 3(b), the calculated photoabsorption cross section is in excellent agreement for the high-energy peak, but the low-energy peak is much lower and broader, and in better agreement with experiment.

Also shown in Fig. 3(a) is the direct $5d$ photoionization spectrum calculated in the absence of any discrete excitations. It is clear that interference with the discrete excitations significantly increases the photoionization cross section. It also emerges that some of the excitations merged within the low-energy peak lie below all calculated thresholds, indicating that discrete $5d \rightarrow 5f$ transitions are involved to some extent in the $5d$ photoabsorption process, but no strong assertions can be made based on these calculations alone. Additional insight into the nature of the $5d$ photoabsorption process was gained from photoion measurements carried out at the BESSY-I synchrotron radiation facility. The summed photoion yield is compared to the photoabsorption data in Fig. 4(a) while individual U^+, U^{2+}, and U^{3+} photoion spectra are displayed in Fig. 4(b). No U^{4+} signal could be detected. The summed photoion yield coincides almost exactly with the photoabsorption data. Although the features of each of the ion yield spectra are broadly the same, the minor differences are significant. All spectra peak at 97.5 eV (as does the photoabsorption spectrum), but the high-energy peak in the U^+ spectrum occurs at an energy of 108 eV while the U^{2+} and U^{3+} spectra peak at 111 eV; the photoabsorption spectrum peaks at 110 eV. Moreover, the U^{3+} spectrum exhibits a minor peak at 93 eV not present in any of the other spectra.

The fact that there is a significant U^+ photoion yield provides further evidence that the character of the $5d$ excitation is at least partly discrete. To elucidate this point we have illustrated in Fig. 5 the possible excitation and decay paths leading to a U^+ final ionic state: (i) through direct photoionization of a $5f$ electron; (ii) through a discrete $5d$-$5f$ excitation with subsequent $5f^{-2}$ super-Coster-Kronig (SCK) decay [28]; (iii) through direct $5d$ photoionization followed by radiative decay. The latter process is not expected to make a significant contribution. Thus the U^+ state is attainable only

TABLE II. The initial and final states used to calculate the photoabsorption spectrum of atomic uranium in the region of the $5d$ excitations. The two-hole notation in the second column denotes autoionization from the $5d^9 6s^2 6p^6 5f^4 6d 7s^2$ state whereby one of the electrons fills the $5d$ core hole while the other is ejected.

Type of configuration	Transition(s)	Configuration(s)
Initial states		$5d^{10}6s^2 6p^6 5f^3 6d 7s^2$
Discrete excited states	$5d \rightarrow 5f$	$5d^9 6s^2 6p^6 5f^4 6d 7s^2$
Direct $5d$ ionization	$5d \rightarrow \varepsilon p,f$	$5d^9 6s^2 6p^6 5f^3 6d 7s^2 + \varepsilon p,f$
Autoionization	$5f^{-2}$	$5d^{10}6s^2 6p^6 5f^2 6d 7s^2 + \varepsilon d,g$
	$6d^{-1}7s^{-1}$	$5d^{10}6s^2 6p^6 5f^4 7s + \varepsilon s,d,g$
	$6p^{-2}$	$5d^{10}6s^2 6p^4 5f^4 6d 7s^2 + \varepsilon s,d,g$
	$6s^{-2}$	$5d^{10}6p^6 5f^4 6d 7s^2 + \varepsilon s,d,g$
	$6s^{-1}6d^{-1}$	$5d^{10}6s^1 6p^6 5f^4 7s^2 + \varepsilon s,d,g$
	$5f^{-1}6d^{-1}$	$5d^{10}6s^2 6p^6 5f^3 7s^2 + \varepsilon p,f$
	$5f^{-1}7s^{-1}$	$5d^{10}6s^2 6p^6 5f^3 6d 7s + \varepsilon p,f$
	$6p^{-1}6d^{-1}$	$5d^{10}6s^2 6p^5 5f^4 7s^2 + \varepsilon p,f$

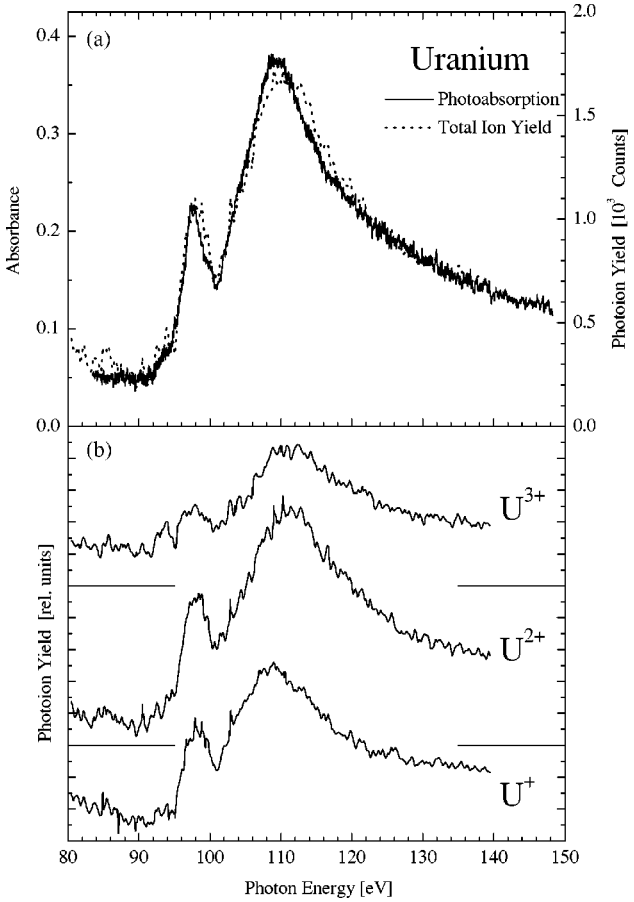

FIG. 4. Experimental photoabsorption and photoion yield spectra of atomic uranium in the $5d$ region: (a) summed photoion yield and photoabsorption spectra; (b) U^+, U^{2+}, and U^{3+} photoion yields.

through the interference of $5d$ excitation to a bound state interfering with the direct $5f$ photoionization channel.

Although in a single-electron picture one would expect $5f^{-2}$ SCK decay to be the dominant channel, the many-body nature of the problem makes all $(5f6s6p)^{-2}$ decay channels important. Since the latter channels may decay to doubly and triply ionized states, discrete excitation also contributes significantly to the U^{2+} and U^{3+} yields. On the other hand, U^{4+} is unlikely to be produced as a result of $5d\rightarrow 5f$ excitation. The absence of a measurable U^{4+} yield is therefore indicative that discrete excitation dominates and hence that the $5f$ wave function has collapsed into the inner well. However, some caution is warranted here. Calculations have revealed that the actinide f potential wells are deeper while the potential barriers are lower than their lanthanide counterparts [29], thus making the barrier less confining. In addition, due to the fact that the $5f$ wave function possesses an extra node, it is by its very nature less localized than a $4f$ wave function, and the outer loop in the wave function is likely to mimic the εf wave function [7]. For this reason the $5f$ wave function can

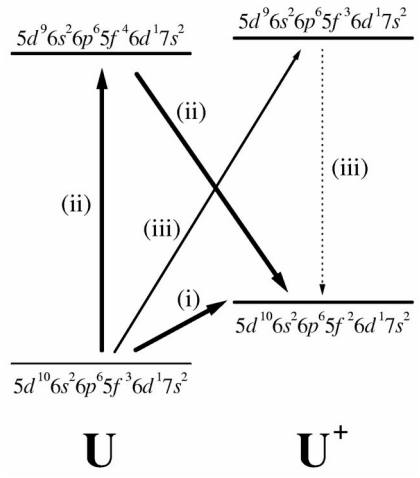

FIG. 5. Direct and indirect paths to the U^+ $5d^{10}6s^26p^65f^26d7s^2$ final state following photoexcitation: (i) direct $5f$ photoionization; (ii) $5d\rightarrow 5f$ excitation followed by SCK decay; (iii) $5d$ ionization followed by radiative decay.

participate in bonding in solid uranium [30] even though it is essentially collapsed in atomic uranium. (The same applies for the $6d$ wave function.) Indeed, from the slightly different shapes and peak shifts towards higher energies for the U^{2+} and U^{3+} yields we infer that a continuum excitation channel must also be available. Hence the resonance should be described as $5d\rightarrow(5,\varepsilon)f$. Establishing the relative strengths of the direct and continuum excitations requires photoelectron data of atomic uranium which are not yet available.

IV. CONCLUSIONS

We have measured and interpreted the photoabsorption spectrum of atomic uranium in the 15–150-eV region covering the range of the strong $6p\rightarrow 6d$ and $5d\rightarrow(5,\varepsilon)f$ excitations. Two structures associated with $6p$ excitations were shown to be discrete in nature and dominated by spin-orbit splitting. Each of the structures is made up from many unresolved transitions between electrostatically split terms. The $5d\rightarrow(5,\varepsilon)f$ excitations, by contrast, are not exclusively spin-orbit split and must be discussed within an intermediate coupling scheme. Additional photoion data give evidence that these excitations are mainly discrete; they also indicate that the $5f$ wave functions in the actinides cannot be treated as the direct equivalent to the $4f$ wave functions in the lanthanide sequence.

ACKNOWLEDGMENTS

We thank Enterprise Ireland and the Deutsche Forschungsgemeinschaft (DFG) for their financial support. We also acknowledge the help of Dietmar Haase at BESSY-I. One of the authors (Ch.G.) would like to thank the Centre for Laser Plasma Research at DCU for their hospitality during his productive and pleasant stay.

[1] R. G. Haire, J. Alloys Compd. **223**, 185 (1995).
[2] O. Meighan, L. Dardis, E. T. Kennedy, T. J. Morgan, J.-P. Mosnier, P. van Kampen, and J. T. Costello, J. Phys. B **32**, L285 (1999).
[3] P. K. Carroll and J. T. Costello, Phys. Rev. Lett. **57**, 1581 (1986).
[4] M. Pantelouris and J. P. Connerade, J. Phys. B **16**, L23 (1983).
[5] P. K. Carroll and J. T. Costello, J. Phys. B **20**, L201 (1987).
[6] M. Cukier, B. Gauthé, and C. Wehenkel, J. Phys. (France) **41**, 603 (1980).
[7] J. P. Connerade, M. W. D. Mansfield, M. Cukier, and M. Pantelouris, J. Phys. B **13**, L235 (1980).
[8] J. P. Connerade, M. Pantelouris, M. A. Baig, M. A. P. Martin, and M. Cukier, J. Phys. B **13**, L357 (1980).
[9] J. Blaise and J.-F. Wyart, *Energy Levels and Atomic Spectra of Actinides* (Pergamon, New York, 1992).
[10] J. C. Fuggle, A. F. Burr, L. M. Watson, D. J. Fabian, and W. Lang, J. Phys. F: Met. Phys. **4**, 335 (1974).
[11] C. Wehenkel and B. Gauthé, Opt. Commun. **11**, 64 (1974).
[12] M. Cukier, P. Dhez, B. Gauthé, P. Jaeglé, Cl. Wehenkel, and F. Combet Farnoux, J. Phys. (France) **39**, L315 (1978).
[13] G. Wendin, Phys. Rev. Lett. **53**, 724 (1984).
[14] G. Wendin and N. Kerr del Grande, Phys. Scr. **32**, 286 (1985).
[15] A. Zangwill and D. A. Liberman, Phys. Rev. B **36**, 6705 (1987).
[16] F. H. Mies, Phys. Rev. **175**, 164 (1968).
[17] P. K. Carroll and E. T. Kennedy, Phys. Rev. Lett. **38**, 1068 (1977).
[18] J. T. Costello, E. T. Kennedy, J.-P. Mosnier, P. K. Carroll, and G. O'Sullivan, Phys. Scr. **T34**, 77 (1991).
[19] P. Nicolosi, E. Jannitti, and G. Tondello, J. Phys. IV **1**, 89 (1991).
[20] E. T. Kennedy, J. T. Costello, J.-P. Mosnier, A. A. Cafolla, M. Collins, L. Kiernan, U. Köble, M. H. Sayyad, M. Shaw, B. F. Sonntag, and R. Barchewitz, Opt. Eng. (Bellingham) **33**, 3984 (1994).
[21] K. J. Ross and B. Sonntag, Rev. Sci. Instrum. **66**, 4409 (1995).
[22] W. Wiley and I. McLaren, Rev. Sci. Instrum. **26**, 1150 (1955).
[23] R. D. Cowan, *Theory of Atomic Structure and Spectra* (University of California Press, Berkeley, 1981).
[24] U. Fano, Phys. Rev. **124**, 1866 (1961).
[25] D. H. Tracy, Proc. R. Soc. London, Ser. A **357**, 485 (1977).
[26] Ch. Gerth, B. Kanngießer, M. Martins, P. Sladeczek, K. Tiedtke, and P. Zimmermann, Eur. Phys. J. D **5**, 65 (1999).
[27] Ba: T. B. Lucatorto, T. J. McIlrath, J. Sugar, and S. M. Jounger, Phys. Rev. Lett. **47**, 1124 (1981); M. Richter, M. Meyer, M. Pahler, T. Prescher, E. v. Raven, B. Sonntag, and H. E. Wetzel, Phys. Rev. A **39**, 5666 (1989). Xe: U. Becker, D. Szostak, H.-G. Kerkhoff, M. Kupsch, B. Langer, R. Wehlitz, A. Yagishita, and T. Hayaishi, *ibid.* **39**, 3902 (1989). Xe, Cs, Ba: T. Nagata, M. Yoshino, T. Hayaishi, Y. Itikawa, Y. Itoh, T. Koizumi, T. Matsuo, Y. Sato, E. Shigemasa, Y. Takizawa, and A. Yagishita, Phys. Scr. **41**, 47 (1990).
[28] D. Coster and R. Kronig, Physica (Utrecht) **2**, 13 (1935).
[29] S. A. Kucas and A. V. Karosene, Litov. Fiz. Sb. **21**, 66 (1981).
[30] B. Johansson and H. L. Skriver, J. Magn. Magn. Mater. **29**, 217 (1982).